


Review

A Review of Non-Linear Optical Imaging Techniques for Cancer Detection

Francisco J. Ávila 

Departamento de Física Aplicada, Facultad de Ciencias, Universidad de Zaragoza, 50009 Zaragoza, Spain; avila@unizar.es

Abstract: The World Health Organization (WHO) cancer agency predicts that more than 35 million cases of cancer will be experienced in 2050, a 77% increase over the 2022 estimate. Currently, the main cancers diagnosed are breast, lung, and colorectal. There is no standardized tool for cancer diagnoses; initially, clinical procedures are guided by the patient symptoms and usually involve biochemical blood tests, imaging, and biopsy. Label-free non-linear optical approaches are promising tools for tumor imaging, due to their inherent non-invasive biosafe contrast mechanisms and the ability to monitor collagen-related disorders, and biochemical and metabolic changes during cancer progression. In this review, the main non-linear microscopy techniques are discussed, according to three main contrast mechanisms: biochemical, metabolic, and structural imaging.

Keywords: cancer; tumor tissue; spontaneous Raman scattering; stimulated Raman scattering; coherent anti-stokes Raman scattering; two-photon excitation; lifetime two-photon fluorescence; two-photon photodynamic therapy; transient absorption microscopy; second harmonic generation; third harmonic generation

1. Introduction

The prognosis of cancer depends mainly on early detection, the type of tumor, treatments outcomes, and genetic factors [1]. Tumor markers help diagnose the type and stage of cancer, and to decide which treatment might be effective. Tumor markers also inform about aggressiveness, whether the treatment is effective, or whether the cancer has recurred. However, tumor markers are not universal for each type of cancer, and the same type of tumor marker can show various expression levels, even in two patients with the same stage and type of cancer.

In contrast, cancer cells share common characteristics such as activation, metabolism and dynamic nuclear activity [2]. Tumors require a microenvironment conducive to tumorigenesis. As a consequence, the extracellular matrix undergoes remodeling through tumor cell-matrix interaction that favors progression and metastasis [3].

Non-linear optical microscopy techniques, such as Raman techniques (i.e., stimulated coherent and anti-stokes Raman scattering) [4] and multiphoton microscopy [5], provide powerful tools for cancer detection and diagnosis. Their ability for deep tissue imaging with high-resolution and minimal photo-damage capabilities makes them invaluable in both research and clinical settings. These techniques enable the visualization of structural [6], biochemical [7], and molecular [8] changes in tissues, offering insights into cancer development, progression, and treatment response.

Traditional immunofluorescence microscopy and spectroscopy techniques in oncology require fluorescent dyes that may interfere with the metabolism of cancer cells [9].

Such limitations are overcome with the label-free nature of the reviewed techniques due to their inherent contrast mechanisms. Furthermore, the potential over other non-linear techniques lies in the ability to be combined with each other, providing joint biochemical, metabolic, and structural information on the same sample under study [10,11]. In this



Citation: Ávila, F.J. A Review of Non-Linear Optical Imaging Techniques for Cancer Detection. *Optics* **2024**, *5*, 416–433. <https://doi.org/10.3390/opt5040031>

Academic Editor: Thomas Seeger

Received: 10 September 2024

Revised: 4 October 2024

Accepted: 14 October 2024

Published: 16 October 2024



Copyright: © 2024 by the author. Licensee MDPI, Basel, Switzerland. This article is an open access article distributed under the terms and conditions of the Creative Commons Attribution (CC BY) license (<https://creativecommons.org/licenses/by/4.0/>).

review, major advances in non-linear optical imaging modalities that provide chemical, structural, and metabolic information about tumor tissues are discussed.

In particular, the operating principles and applications in cancer detection for biochemical (spontaneous, stimulated and coherent anti-stokes Raman scattering), metabolic (two-photon excitation microscopy, lifetime fluorescence microscopy and transient absorption microscopy), and structural (second and third-harmonic generation microscopy) imaging techniques are analyzed.

2. Biochemical Imaging

2.1. Spontaneous Raman Scattering

Although spontaneous Raman scattering is not a non-linear but a linear effect, it has been added to this section for a better understanding of the principles of non-linear Raman techniques as described in Sections 2.2 and 2.3.

2.1.1. Principle

Raman spectroscopy is an optical scattering imaging technique that provides non-destructive analysis of the chemical structure of biological tissues [4]. Raman scattering occurs upon the interaction of high-power lasers with the chemical bonds composing the biological sample. The Raman scattered light undergoes a wavelength shift of the incident light whose intensity and spectrum depend on the vibrational (chemical) bond of the specific molecules. Figure 1 schematizes the Raman scattering principle: During an elastic scattering event, the energy of the molecule would not change, and therefore, the scattered light retains the wavelength of the incident source (i.e., Rayleigh scattering). However, a Raman event is an inelastic scattering process in which an energy transfer occurs between the molecule and the scattered photons. If during the light-matter interaction the molecule is excited to a higher vibrational state (i.e., the molecule gains energy) the process is called Stokes Raman scattering. Conversely, if the molecule is relaxed to a lower vibrational state, the scattered photons gain energy with decreasing wavelength; this process is known as anti-Stokes Raman scattering [12].

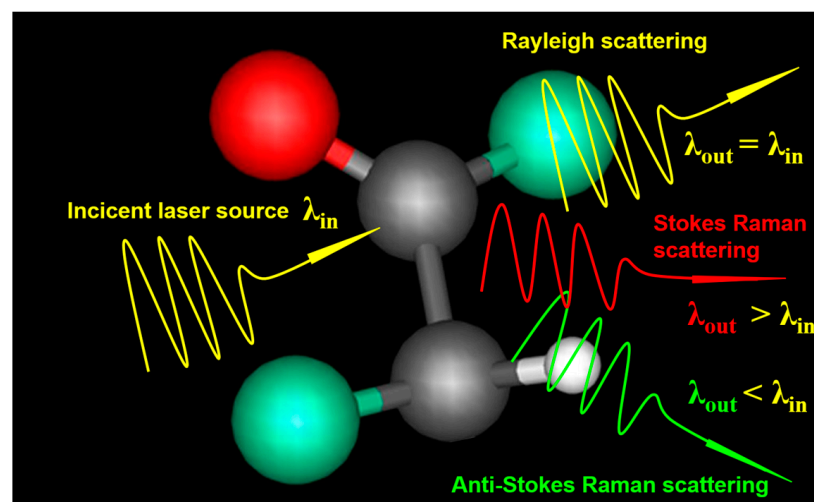


Figure 1. Raman scattering principle.

Raman scattering shift is related to the vibrational state of the constituent atoms, where the interaction of the external electric field $\vec{E} = E_0 \cos(\omega_0 t)$ (i.e., the laser source), with the specimen at the atomic scale induces a dipole moment (\vec{P}) that defines the polarizability ($\vec{\alpha}$) as [13]:

$$\bar{\alpha} = \frac{\vec{P}}{\vec{E}} \quad (1)$$

If the molecular polarizability is expanded into a Taylor series to the first order for a generalized coordinate $r = r_0 \cos(\omega_0 t)$, which is expressed as follows:

$$\bar{\alpha}(r) = \bar{\alpha}_0 + \left(\frac{\partial \bar{\alpha}}{\partial r} \right)_0 + \dots \quad (2)$$

The scattered electric field \vec{E}_{scatt} proportional to the induced dipole moment can be expressed as follows:

$$\vec{E}_{scatt} = \bar{\alpha}_0 E_0 \cos(\omega_0 t) + 1/2 \left(\frac{\partial \bar{\alpha}}{\partial r} \right)_0 r_0 E_0 [\cos(\omega_0 - \omega)t + \cos(\omega_0 + \omega)t] \quad (3)$$

In Equation (3), the first term corresponds to elastic (Rayleigh) scattering. The second term represents the Raman scattering effect, where the shift frequencies $(\omega_0 - \omega)$ and $(\omega_0 + \omega)$ correspond to the Stokes and anti-Stokes Raman processes.

2.1.2. Applications in Cancer Detection

The contrast mechanism of Raman spectroscopy lies in the differences between the wavelength of incident and scattered light. Furthermore, Raman scattering is a label-free optical technology that is sensitive to changes in cells and macromolecules occurring during carcinogenesis; therefore, it is a powerful tool for tumor diagnosis at the molecular level [14,15].

Raman scattering imaging extends classical spectroscopy to 3D visualization of the molecular structure and morphology of tumors [16] and then to the classification of types and subtypes of malignant lesions in cancer diagnosis.

Raman scattering is able to distinguish between normal and cancerous tissues by identifying specific molecular biomarkers. Each tissue type exhibits a unique Raman spectrum based on its molecular constituents, allowing researchers to detect chemical changes indicative of malignancy, such as brain [17] and breast cancer [18,19].

Raman scattering has been employed in surgical settings to provide real-time diagnosis of tumor margins [20]. During cancer surgery, it is crucial to ensure complete removal of the tumor, which typically requires histopathological evaluation by a pathologist. Raman scattering allows for rapid assessment of tissue at the surgical site, potentially reducing waiting time and improving surgical outcomes [21].

The tumor microenvironment plays a critical role in cancer metabolism [22] and progression. Raman scattering can be used to map and analyze the molecular components of the tumor microenvironment, such as the extracellular matrix and infiltrating immune cells. This helps to understand how the environment surrounding the tumor contributes to its growth and resistance to treatment [22].

Raman scattering offers label-free chemical imaging, which has sparked interest in pharmacokinetic research due to the ability to track the biodynamics of anti-cancer drug delivery in real-time [21]. Figure 2a shows the confocal Raman imaging spectra from a human hepatocellular carcinoma cell line (HepG2) in the lipids, cytoplasm, and nucleus regions of the cell. Figure 2b compares the Raman spectra of HepG2 before (green spectrum) and after incubation (dark blue spectrum) with drug delivery polymers based on poly (lactic-co-glycolic acid) nanoparticles (PLGA NPs). The pink spectrum corresponds to the PLGA NPs in the dry state. The cells under study are shown in the insets.

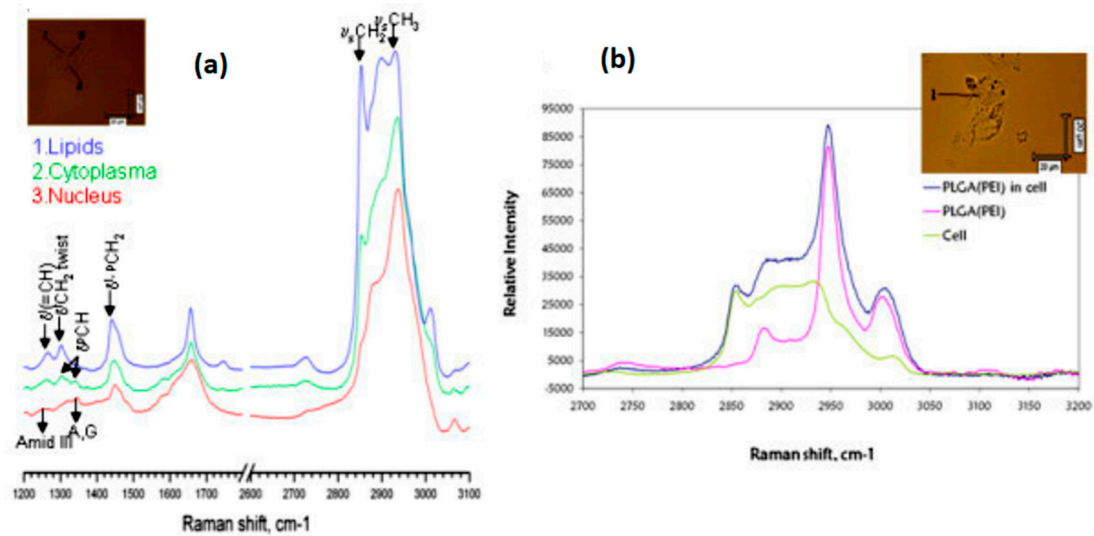


Figure 2. (a): Raman spectra of HepG2 cell line in lipids (blue), cytoplasm (green), and nucleus (red) regions. (b): Comparison of Raman spectra before (green) and after incubation of HepG2 with PLGA nanoparticles (blue). The pink spectrum corresponds to the isolated PLGA NPs. Image reproduced from [23].

2.2. Stimulated Raman Scattering

2.2.1. Principle

While spontaneous Raman scattering is an incoherent process, in stimulated Raman scattering (SRS) a pump and a Stokes photon interact with the tissue, resulting in the coherent generation of a new photon whose frequency is shifted by the vibrational energy of the molecules in the tissue [24].

SRS enhances the weak Raman signals by transferring energy from the pump to the Stokes beam, enabling the detection of molecular fingerprints with higher spatial resolution and faster acquisition times compared to conventional spontaneous Raman scattering [25].

2.2.2. Applications in Cancer Detection

SRS has emerged as a powerful tool for cancer detection due to its ability to provide high-resolution, label-free imaging of biological tissues. SRS takes advantage of the intrinsic vibrational properties of biomolecules, allowing for the identification and differentiation of cancerous cells from normal tissues based on their different molecular signatures [26]. Recently, the SRS technique has been improved by incorporating high-content SRS histology platforms [27] that have been shown to successfully map unsaturated and saturated lipids, extracellular matrix, cellular proteins, and water in breast tissue, and thereby provide both morphological and chemical information on unstained cancer breast tissues.

One of the major advantages of SRS microscopy in cancer detection is its ability to generate real-time in vivo images without the need for exogenous markers and the visualization of tumor margins.

This feature is particularly valuable in complex clinical procedures such as brain tumor surgery [28], ensuring complete removal of cancerous tissue while preserving healthy surrounding tissue [29]. This precise delineation is critical to reducing the likelihood of cancer recurrence and improving patient outcomes.

Recently, focal therapy has been proposed as a way to precisely remove the malignant mass in prostate cancer while preserving surrounding healthy tissue.

This has been made possible by the emergence of real-time histopathological capabilities of artificial intelligence-enhanced SRS [30]. As an example, Figure 3 (left column) shows stimulated Raman histology (SRH) images corresponding to a non-Hodgkin lymphoma specimen, non-small cell lung cancer brain metastasis (b), and glioblastoma specimens. After image acquisition, a trained convolutional neural network (CNN prediction) displays

probability heat maps (middle column) corresponding to the tumor (red), low-quality regions (blue), and regions outside the tumor (green). If the probability maps and SRH are superimposed, the color-coded SRH images can help the surgeon to better interpret the histological information.

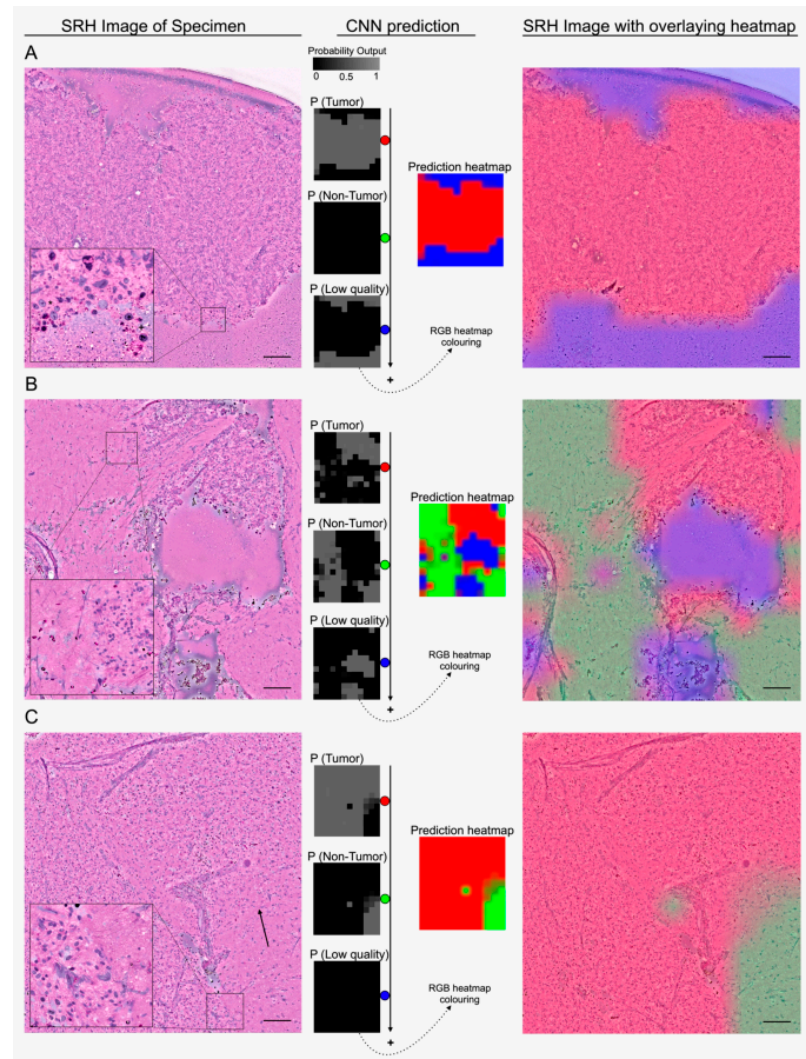


Figure 3. SRH images corresponding to a non-Hodgkin lymphoma specimen (A), non-small cell lung cancer brain metastasis (B), and glioblastoma (C) specimens (left column). Heat maps of CNN prediction algorithm (middle column) and overlay of the SRH images with heat maps are shown in the right column. Scale bar: 100 μm . Image reproduced from [30].

2.3. Coherent Anti-Stokes Raman Scattering

2.3.1. Principle

Stimulated Raman scattering and coherent anti-Stokes Raman scattering (CARS) are non-linear optical methods used in vibrational spectroscopy but with different signal generation mechanisms and biomedical applications.

While in SRS, the signal is generated when the energy difference between a pump and a Stokes laser beam matches the vibrational frequency of a molecular bond, CARS generates a new frequency at the anti-Stokes wavelength after the interaction between the pump and Stokes beams. This new signal is a coherent light wave at a frequency that is the sum of the pump frequency and the vibrational frequency of the sample [31].

In CARS, the generated coherent signal is amplified along the propagation direction of the incident beams, allowing high-contrast three-dimensional biochemical imaging [32].

CARS provides stronger signals and the ability to suppress non-resonant fluorescence background signals, making it suitable for applications in biomedical imaging and materials science [33,34].

Furthermore, the incorporation of polarization units into CARS microscopes has made it possible to make the intensity of the anti-Stokes radiation sensitive to the directionality of molecular bonds and then add molecular orientation sensitivity to the regular chemical information of CARS microscopy [35]. These polarimetric approaches added new capabilities to CARS microscopy allowing for the determination of Raman polarization ratios and to study those polarization-sensitive features in CARS spectra from biological specimens [36].

2.3.2. Applications in Cancer Detection

CARS microscopy has emerged as a powerful tool in neuroscience and cancer research due to its ability to provide a coherent signal of vibrational signatures that are also characteristics of specific chemical bonds of biomolecules [37]. Lipid-rich tumor tissues have been related to cancer metastasis; however, if the role of lipids in carcinogenesis is not well understood, lipid-rich tumors cannot be distinguished from carcinoma. One of the potentials of CARS imaging is to visualize the intracellular lipid aggregation in tumor cells [38]. Furthermore, CARS microscopy has been employed to detect circulating tumor cells in the peripheral blood of metastatic patients [39]. Then, the subcellular information provided by CARS microscopy has helped to reveal metabolism in cancer progression [22] and anti-cancer drugs [40].

As an example, Figure 4 shows the ability of CARS microscopy to image cancer cells and their main sub-cellular components. Figure 4a maps the intracellular distribution of nucleic acid (blue), proteins (green), and lipids (red) from a HepG2 cancer cell line. The corresponding CARS spectra are shown in Figure 4b.

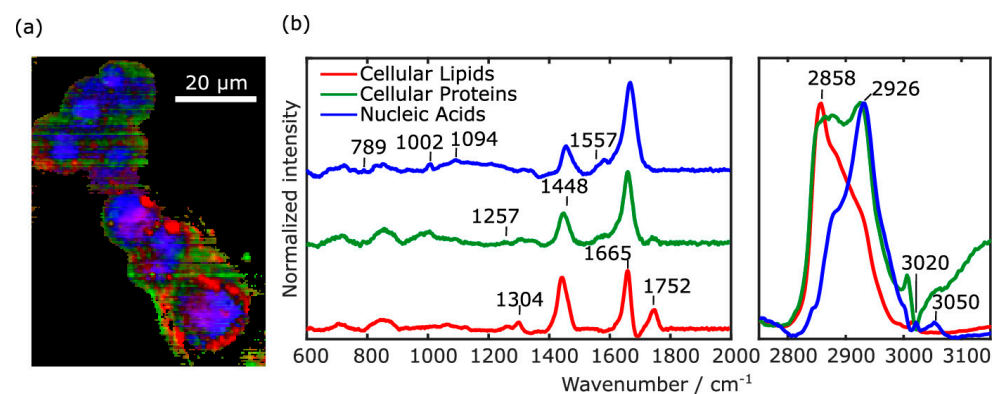


Figure 4. (a): CARS image of HepG2 cell line showing lipids (red), proteins (green), and nucleic acid (blue) regions. (b): associated CARS spectra. Image reproduced from [41].

3. Metabolic Imaging

3.1. Two-Photon Excitation Fluorescence Microscopy

3.1.1. Principle

Multiphoton imaging arises from the second and third-order non-linear interaction between a high-power ultrafast infrared pulsed laser (traditionally titanium–sapphire lasers) and biological tissues [42]. When the addition of the energy of two or more photons allows the ground fluorophore to be excited to a higher energy excitation state, an electronic transition occurs in a manner similar to regular fluorescence [43] (single photon absorption). Biological molecules in the excited state then fall back to the ground state with spontaneous emission of a photon of lower energy than the sum of the incident photons due to the non-radiative vibrational relaxation process. If two photons are absorbed, the process is known as two-photon excitation fluorescence (TPEF) and has the ability to produce endogenous excitation fluorescence from biomolecules such as lipofuscin, melanin, flavin, and NADPH [44].

In multiphoton imaging, the excitation is confined to a focal volume where the scattered light is inversely proportional to the fourth power of the wavelength of the excitation source. Furthermore, the emission intensity of endogenous fluorophores is proportional to the square of the excitation source; these particular features provide the multiphoton imaging modality with intrinsic optical sectioning capabilities and high penetration power within scattering tissues [45].

Since the experimental demonstration of the suitability of two-photon excitation fluorescence (TPEF) for biological imaging in the 1990s [46], TPEF microscopy has been employed for deep tissue imaging [47], functional imaging in neurons [48], studying the dynamics of stromal cells interaction [49], or intravital subcellular imaging [50]. Subsequently, applications of TPEF microscopy in tumor research have been expanded to tumor microenvironment, metabolism, angiogenesis, and metastasis [51].

3.1.2. Applications in Cancer Detection

In some types of malignancies, the diagnosis often comes at a very late stage such as gastric cancer [52]. Diagnosis of gastric cancer is made by visual assessment of gastrointestinal endoscopy and late confirmation by histopathology. However, misinterpretation in the former (endoscopy) due to the lack of obvious signs by the naked eye, may cause a late impact in the latter (histopathology). In that sense, TPEF microscopy enables the discrimination of normal gastric tissue from cancer, adenoma, or ulcers due to the capabilities of two-photon imaging to visualize and measure enzymatic activity [53].

Cancer-associated fibroblasts (CAF) are cells within the tumor that promote cancer proliferation and extracellular matrix remodeling [54]. They are one of the major stromal cell populations in solid tumors and contribute to drug resistance [55]. In that regard, TPEF microscopy has demonstrated the potential to analyze the structure and spatial organization of gastric cancer cells and monitor spheroid growth. Figure 5 shows a single plane of TPEF images of a bicellular spheroid acquired six days after the start of growth.

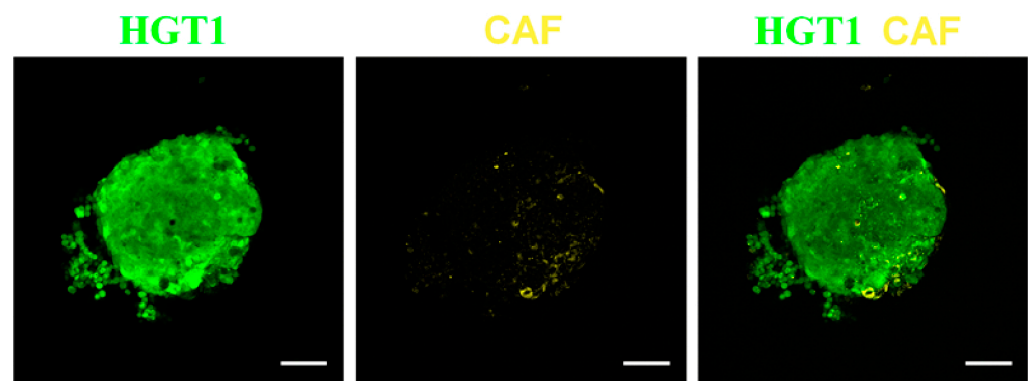


Figure 5. TPEF image of CAF (**middle**); monocellular HGT1 (labeled with eGFP) spheroids (**left**) and bicellular HGT1/CAF (**right**). Scale bar: 100 μ m. Image reproduced from [55].

Pathological assessment (i.e., histopathology) of treatment response requires tedious and time-consuming labeling processes. As a label-free imaging technique, TPEF microscopy enables the evaluation of histopathological changes induced by neoadjuvant therapy in the preoperative stage, revealing residual tumoral cells, fibrotic reactions, and inflammatory cell infiltration [56].

Tumor cells invade adjacent tissues by secreting degradative enzymes that reduce the pH of lysosomes, and then the extracellular pH of tumor tissues becomes acidic. TPEF microscopy has been shown to be pH-sensitive in the case of human colon cancer [57].

Photodynamic therapy (PDT) is a modern non-invasive light-matter-based interaction method that uses photosensitizers or light-activated drugs for the treatment of non-malignant diseases and various types of cancer [58].

Once the photosensitizers are activated by a selective wavelength, a process of selective destruction of malignant or abnormal cells begins.

One of the main limitations of PDT was the photodamage induced by single-photon excitation of the photosensitizers; however, the application of the concept of two-photon absorption made it possible to overcome this medical limitation due to the negligible photo-toxicity of the non-linear process that makes the technique suitable for the study of living cells [59].

The combination of two-photon excitation (TPE) and PDT gave rise to a new therapy concept (TPE-PDT) with greater penetration power in biological tissue and reduction of cell phototoxicity with promising therapeutic applications in the treatment of tumors [60].

PDT can destroy cancerous cells in inoperable types of cancer [61] or before tumors spread. PDT has demonstrated effectiveness in the treatment of colorectal [62], lung [63], breast, liver, and pancreatic cancer [64]. The main therapeutic mechanisms of PDT are immune response, vascular damage, and direct destruction of cancer cells.

TPEF lifetime microscopy measures the fluorescence decay of endogenous (or exogenous) fluorophore emission, allowing for label-free in-vivo imaging of metabolic dynamics [65] with promising applications in infectious, neurodegenerative, and cancer diseases [66].

In particular, the characterization of NAD(P)H fluorescence lifetime has been shown to be an intrinsic biomarker of the cellular metabolic state of living tissues, capable of tracking tumor cell dynamics [67].

In a recent publication reported by Karrobi et al. [68], lifetime TPEF microscopy was used to investigate changes in the cellular metabolism of breast spheroids, including non-cancerous epithelial breast (MCF-10A) and breast cancer (MD-MB-231) cell spheroid lines embedded in collagen. The findings revealed a greater shift in cancer spheroids towards oxidative phosphorylation and how they invaded collagen over time with stronger metabolic gradient modifications than MCF-10A spheroids.

Figure 6 shows an example of a time-integrated NAD(P)H two-photon excitation fluorescence image from a non-cancerous epithelial breast cell spheroid line (a) and the representative fluorescence decay signal (b).

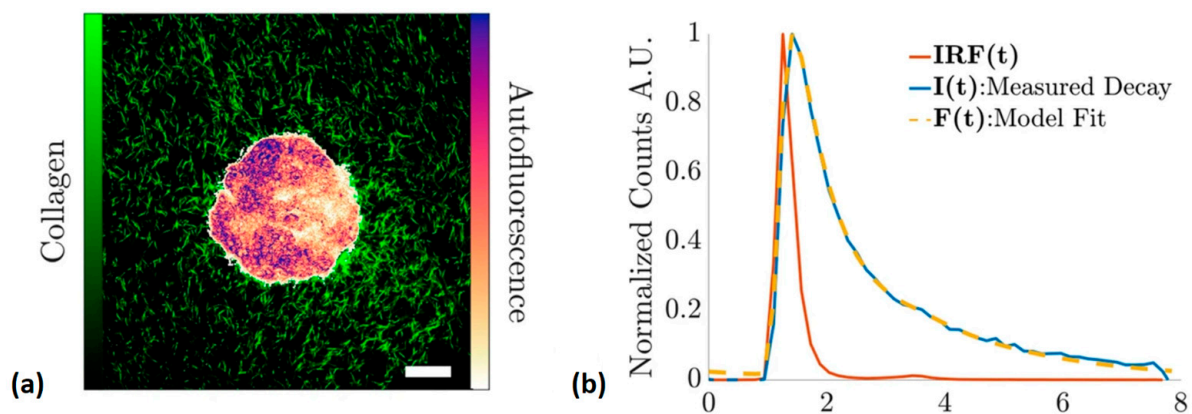


Figure 6. Lifetime TPEF image of a normal breast cell (a) and the normalized fluorescence decay signal (b). $I(t)$, $IRF(t)$, and $F(t)$ correspond to the intensity of the decay signal, the impulse response function, and a model fitted, respectively. Reproduced from [68].

3.2. Transient Absorption Microscopy

3.2.1. Principle

Transient absorption microscopy (TAM) is an advanced non-linear optical technique used in biology to study biodynamical processes at the subcellular scale with high spatiotemporal resolution. TAM works by probing changes in the absorption of light by a sample after being excited by a short laser pulse, allowing real-time observation of changes

in the electronic states of molecules and providing information about fast processes such as energy transfer, charge separation, or molecular dynamics [69].

TAM can be employed for the study of photosynthetic processes, protein dynamics, and the behavior of chromophores and fluorophores within cells. For instance, it has been used to investigate how light energy is converted into chemical energy in photosynthesis, revealing key details about the lifetimes and pathways of excited states in complex biological systems [70].

Overall, transient absorption microscopy provides a unique window into the ultrafast dynamics of biological systems, offering detailed information crucial for unraveling the mechanisms underlying various biological functions [71].

3.2.2. Applications in Cancer Detection

In cancer detection, TAM is particularly useful for identifying molecular signatures that distinguish cancerous cells from healthy ones. For example, TAM can detect differences in the electronic states of chromophores and other biomolecules associated with cancer, such as mitochondrial redox, and then provide insights into the metabolic and structural changes that occur during neurodegenerative diseases, diabetes, or cancer [72]. Additionally, TAM has been used to study the dynamics of photosensitizers in photodynamic therapy (PDT), a cancer treatment that relies on light-activated compounds to kill cancer cells. By monitoring the transient absorption signals of these photosensitizers, researchers can optimize PDT treatment protocols and improve the efficacy of cancer therapy [73].

One of the most recent studies published by Xin and coworkers [74], showed the power of combining stimulated Raman scattering and transient absorption microscopy for real-time observation of subcellular components (i.e., proteins, lipids, and DNA). Their findings revealed induced oxidative damage in a single live cancer cell during PDT.

4. Structural Imaging

4.1. Second Harmonic Generation

Cancer cells are responsible for tumor growth and migration to other organs; however, the extracellular matrix undergoes remodeling that promotes the progression of metastasis and tumorigenesis [75]. The next subsection discusses the “gold standard” non-linear imaging modality to visualize the extracellular matrix primarily composed of collagen [76].

4.1.1. Principle

Multiphoton microscopy is sensitive to harmonic generations, where two or three incident photons can be instantaneously converted into a single photon with half or one-third of the excitation wavelength giving rise to second and third harmonic generation microscopy (SHG and THG), respectively [77]. Those frequency conversions are not absorptive processes and occur without energy dissipation as a result of excitation photons summation and phase matching induced by the non-linear susceptibility of the biological structures [78].

The contrast mechanism of SHG and THG microscopy, unlike TPEF which requires endogenous fluorophores, arises from the frequency conversion of the incident photons due to the non-linearity of the electromagnetic response of the specific molecular structures of biological tissues. According to the non-linear optics theory, the excited non-linear polarization (\vec{P}) is related to the excitation laser source by means of the non-linear susceptibility, $\hat{\chi}^{(n)}$ [79]:

$$\vec{P} = \epsilon_0 + \hat{\chi}^{(1)} \cdot \vec{E} + \hat{\chi}^{(2)} \cdot \vec{E}\vec{E} + \hat{\chi}^{(3)} \cdot \vec{E}\vec{E}\vec{E} + \dots \quad (4)$$

Therefore, the generation of harmonics depends not only on the need for ultrafast and intense pulsed laser but also on the non-linear susceptibility of the biological tissues. The SHG signal is provided only in non-centrosymmetric media such as fibrillar collagen [80]. In contrast, THG arises from sources such as lipid-water interfaces [81] and myelinated axons [82]. Figure 7 schematizes the main multiphoton imaging modalities, which provide

label-free three-dimensional visualizations of biological structures at the cellular level with negligible phototoxicity. These features make multiphoton microscopy a potential tool for the analysis of tumor lesions.

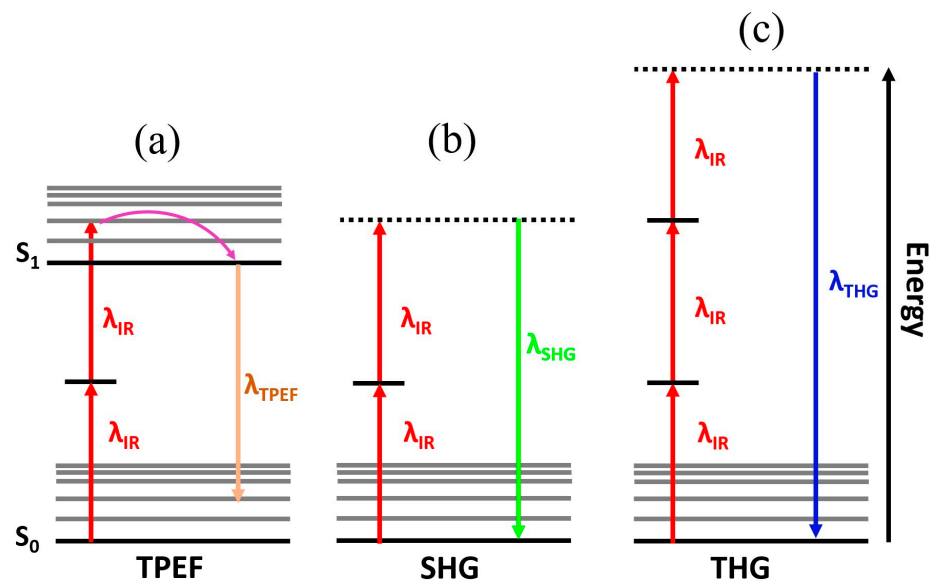


Figure 7. Illustration of the two-photon excitation fluorescence (a), second harmonic generation (b), and third harmonic generation (c) non-linear processes.

The extracellular matrix is not only responsible for cell maintenance, but also for cell migration and proliferation [83]. In the extracellular matrix (ECM) of connective tissues, collagen is the most abundant protein and plays a fundamental role in functional structure and cellular processes [84].

Type-I fibrillar collagen is organized in a non-centrosymmetric molecular structure and possesses strong non-linear susceptibility. Nowadays, second harmonic generation (SHG) microscopy (see Figure 6b for the illustration of the SHG concept) is considered the gold standard imaging technique for visualizing and characterizing collagen-formed tissues [85]. The SHG signal is endogenous; therefore, the contrast mechanism arises from the structure of the sample, making this imaging technique sensitive to the molecular structure of the collagen-based connective tissue [86].

Beyond collagen-based tissues, SHG microscopy allows visualization of the structural proteins [86], membrane potential in neurons [87], or myosin filaments [88] when combining SHG and TPEF microscopy.

The SHG signal is a coherent process of tensorial nature in which forward (F-SHG) and backward (B-SHG) emissions coexist; the ratio of F/B-SHG depends on the structure of the susceptibility tensor [89]. Therefore, SHG imaging is a powerful optical microscopy technique to analyze collagen disorders (remodeling) associated to cancer and fibrous connective tissues [90].

4.1.2. Applications in Cancer Detection

In cancer progression, the extracellular matrix is remodeled alongside abnormal cell growth [91]. In particular, collagen undergoes fibrillation that induces increased stiffness in the ECM and promotes angiogenesis and cancer invasion [92]. Furthermore, changes in SHG directionality emission (i.e., the F/B-SHG ratio) have been found to be altered in the tumor bulk but not at the stroma interface [93], where high values of the F/B-SHG ratio describe highly organized ECM tissues.

Therefore, the characterization of spatial remodeling of collagen in the ECM is crucial as tumor invasion and metastasis are facilitated by alterations in the ECM [94].

SHG microscopy images from collagen fibers require quantitative analysis to first detect alteration in the spatial patterns and then numerically compute the collagen remodel-

eling and degree of organization. The structure tensor, fast Fourier transform, Wavelet, or Hough transforms are well-established image transformation methods from which structural information can be extracted. An overview of the main image processing techniques for quantitative analysis of SHG imaging can be found in [95].

In particular, the structure tensor [96] has been demonstrated as a useful method to quantify the organization of collagen-based tissues and classify different spatial patterns. The Hough transform was successfully used to discriminate between normal and malignant tissues, analyzing the surrounding collagen of thyroid cancer nodule capsules [97].

The SHG process exhibits a strong polarization dependence [98]. The polarization-sensitive nature of SHG (P-SHG) microscopy has allowed the measurement of the second-order non-linear optical susceptibility tensor [99], providing information about the ultrastructure of collagen. As an example, Figure 8 compares the spatially-resolved components of the non-linear susceptibility tensor in normal and cancerous breast tissues, obtained using P-SHG.

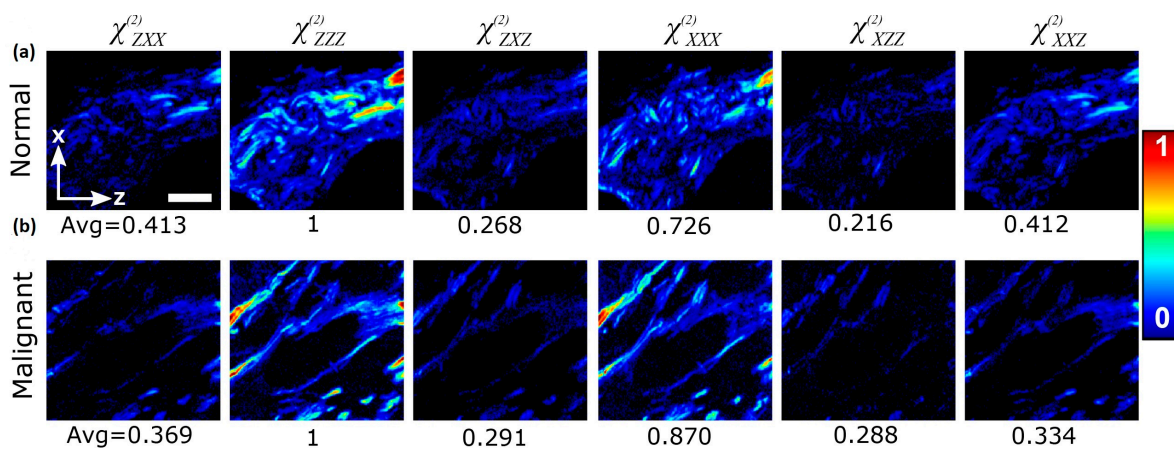


Figure 8. Second-order susceptibility values of normal (a) and tumor breast (b) tissues. Scale bar: 20 μm . Images reproduced from [100].

Tokarz et al. [101] used P-SHG microscopy to calculate the components of the susceptibility tensor from histopathological samples of cancerous thyroid tissues. They were able to measure the molecular chirality of the malignant tissues and found cancer-related collagen disorders at molecular levels.

Polarimetric SHG microscopy reveals collagen orientation and ultrastructure that cannot be accessed by non-polarized SHG imaging. P-SHG has also been used to distinguish between breast, osteosarcoma, liver fibrosis, or melanoma tissues [102–105].

Therefore, pathologists can benefit from the invaluable ultrastructural information provided by polarization-sensitive SHG microscopy.

4.2. Third Harmonic Generation

4.2.1. Principle

While SHG microscopy arises mainly from non-centrosymmetric proteins such as Type-I collagen, the third-harmonic generation (THG) signal originates mainly from interfaces between water and lipid-rich structures such as lipid droplets or membrane lipid layers [106,107]. In this non-linear process, the frequency of the excitation light is tripled after the interaction with biological tissue (see Figure 7c) and provides information about the refractive index discontinuities of material interfaces via the third-order non-linear susceptibility tensor $\chi^{(3)}$ [108].

4.2.2. Applications in Cancer Detection

THG offers structural information of single cells with submicron resolution and intracellular heterogeneities allowing discrimination between benign and tumorous tissues [109].

Gavgiotaki et al. [110] reported quantitative differentiation of malignant cells in benign and tumorous breast biopsies and found how disease severity altered cell morphological information that distinguished cell malignant grade.

Figure 9 shows THG imaging of cells isolated from healthy tissue (left column) and for different grades of breast cancer. The top and bottom rows compare nuclear irregularities and nucleoli heterogeneities. The ability of THG to detect variability in tumor cell size and shape in a non-invasive and label-free manner provides invaluable structural information from cancer biopsies at the subcellular level of resolution.

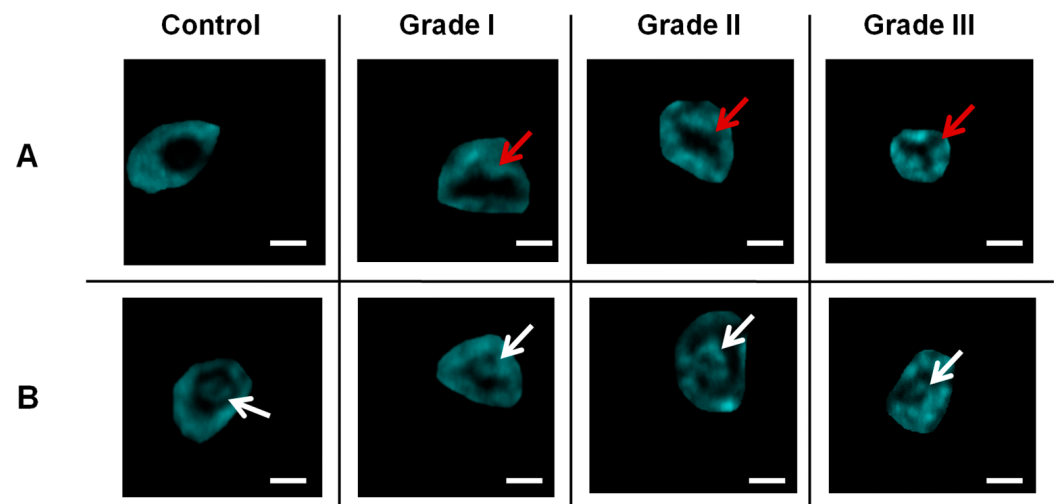


Figure 9. THG images of cells isolated from healthy tissue (left column) and for different grades of breast cancer (third to fourth columns). The top (A) and bottom (B) panels compare the morphology of the nucleus and nucleoli, respectively. Red and white arrows indicate the irregular nucleus and nucleoli, respectively. Scale bar: 2 μm . Images reproduced from [109].

5. Discussion

In this article, the main methods of non-linear optical microscopy were analyzed, considering three different contrast mechanisms: biochemical, metabolic, and structural. Table 1 summarizes the reviewed technique, the principle, the contrast mechanisms, and the main applications, as well as the main advantages and disadvantages.

Cancer cells exhibit non-linear optical properties that can also be considered as a predictive indicator of cellular response induced by the treatment [111]. The emergence of biocompatible nanomaterials has allowed the conversion of macroscopic analysis of tumor tissues to molecular diagnosis tools in cancer research. Nanocluster enables low-toxicity, biocompatible tumor labeling that constitutes optical contrast biomarkers exhibiting non-linear optical properties [112] that can be analyzed with the reviewed optical methods at the cellular and molecular scales. Furthermore, nanoparticles, including gold nanoparticles, protein nanoparticles, cell membrane nanoparticles quantum dots, and others, can be controlled externally by optical methods, magnetism, and enzymes that make them behave like smart nanoparticles that are emerging as the new era of intelligent nanoparticle cancer treatment [113]. Studying the non-linear optical properties of cancer tissues allows for rapid estimation of cellular damage or response to treatments, spatial remodeling of the ECM in cancer growth, and the optimization of two-photon photodynamic therapy [114]. Furthermore, a recent study reported by Hoque et al. [115] reported a promising method to detect cancer by analyzing the non-linear optical properties of blood plasma. Their results achieved an accuracy of 92% in discriminating between normal and cancerous samples.

Table 1. Summary of the reviewed techniques, principles, contrast mechanisms, applications, and key features. RS: spontaneous Raman scattering; SRS: stimulated Raman scattering; CARS: coherent anti-Stokes Raman scattering; TPEF: two-photon excitation fluorescence; FLIM: fluorescence lifetime imaging microscopy; TAM: transient absorption microscopy; SHG: second harmonic generation; THG: third-harmonic generation.

| Technique | Principle | Contrast Mechanism | Applications | Key Features |
|-----------|-------------------------------------------------------------------------------------------------------------|---------------------------------------------------------------------------------|----------------------------------------------------------------------------------------------------------------|------------------------------------------------------------------------------------------------------------------------------------------------------------------------------------------------------------------------|
| RS | Inelastic scattering of light, where energy is transferred to molecular vibrations. | Chemical composition based on vibrational modes. | Chemical imaging, material science, cancer diagnostics. | <ul style="list-style-type: none"> - Weak signal, requires longer acquisition times. - Molecular specificity without labels. - Sensitive to chemical bonds. |
| SRS | Enhanced Raman signal by stimulating Raman-active modes with pump and probe lasers. | Chemical composition based on vibrational modes | Fast imaging of live cells, tissue imaging. | <ul style="list-style-type: none"> - Higher sensitivity than spontaneous Raman. - Rapid, real-time imaging. - Requires synchronized lasers. |
| CARS | Non-linear process where anti-Stokes shifted light is generated, enhancing Raman signal. | Chemical composition based on vibrational modes | Label-free imaging, lipid mapping, biomedical imaging. | <ul style="list-style-type: none"> - High sensitivity, fast imaging. - Non-resonant background can interfere with signals. - Complex instrumentation required. |
| TPEF | Non-linear excitation where two photons are absorbed simultaneously to excite a fluorophore. | Fluorescence emission from excited states | Deep tissue imaging, neuroscience, cellular imaging. | <ul style="list-style-type: none"> - Allows deep tissue penetration. - Reduces photodamage and photobleaching. - Requires pulsed lasers. |
| FLIM | Measures the decay time of fluorescence after two-photon excitation. | Temporal decay of fluorescence signal, independent of intensity. | Cellular metabolism, protein interactions, cancer diagnostics. | <ul style="list-style-type: none"> - Provides functional information. - Requires complex lifetime analysis. - Useful for multiparametric imaging. |
| TAM | Measures the absorption of a probe pulse following excitation by a pump pulse. | Differential absorption signal revealing electronic and vibrational dynamics. | Study of ultrafast dynamics, excited state lifetimes, and charge transfer in materials and biological systems. | <ul style="list-style-type: none"> - High temporal resolution. - Can study non-fluorescent molecules. - Requires ultrafast lasers and sophisticated analysis tools. |
| SHG | Non-linear optical process where two photons combine to form a single photon with twice the energy. | Structural information from non-centrosymmetric molecules (e.g., collagen). | Imaging of collagen, muscle fibers, and other non-centrosymmetric structures. | <ul style="list-style-type: none"> - Label-free imaging. - Specific to non-centrosymmetric structures. - No photobleaching or phototoxicity. |
| THG | Non-linear optical process where three photons combine to form a single photon with three times the energy. | Interface-sensitive imaging of boundaries between different refractive indices. | Imaging of interfaces, cellular structures, and developmental biology. | <ul style="list-style-type: none"> - Label-free, subcellular resolution. - Sensitive to interfaces and material properties. - Limited to specific sample types with clear interfaces. |

6. Conclusions

Cancer cells induce non-linear optical properties in cell-matrix interaction [116] that can be measured from multimodal optical approaches that also provide invaluable monitoring of anti-cancer drugs and support the application of photodynamic therapies and the use of nanomaterials as an emerging paradigm for cancer treatment.

Non-linear optical techniques reviewed in this paper, such as multiphoton microscopy and Raman approaches, are technically sophisticated and their complexity often requires specialized equipment and expertise, limiting their clinical application. Those technical limitations added to elevated costs as well as required training and infrastructure make the implementation of these techniques in hospitals difficult. Thus, non-linear techniques are still confined to research labs and not accessible to clinical practices for diagnostic procedures.

Other limitations of non-linear optical techniques for cancer detection are the penetration depth, the lack of standardization of clinical guidelines, and in-vivo applications, in which motion artifacts, blood flow, and complexity of the tumor environment can alter the image quality and then the diagnostic accuracy.

Those limitations may be substantially addressed by focusing on the recommendations summarized in Table 2.

Table 2. Main limitation and recommendations for future improvements of non-linear optical approaches for cancer detection.

| Limitation | Recommendation |
|---------------------------|--------------------------------------------------------------------------------------------------------------------------------------------------------------------------------------------------------------------|
| High-costs | Cost reduction strategies, including the development of simplified designs based on cost-effective materials, open-sources manufacturing processes. |
| Technological equipment | Development of robust, affordable, and user-friendly systems and data analysis software. Advancements in miniaturizing equipment. |
| Tissue penetration | Enhance tissue penetration depth with the implementation of adaptive optics and the combination with multimodal approaches. |
| Data Analysis | Incorporating artificial intelligence for automatic image processing, pattern recognition, and data analysis to enhance the differentiation of cancerous tissues. |
| In vivo trials | More in vivo studies and clinical trials are needed to demonstrate the efficacy and reliability of non-linear optical techniques in real-clinic cancer detection, to ensure broad applicability. |
| Multi-modal imaging | Combining the contrast mechanisms of the reviewed techniques with other imaging techniques such as PET or MRI could offer a more comprehensive diagnostic approach. |
| Standardization protocols | It is critical to establish standardized protocols for the use of non-linear optical techniques in cancer detection. This includes guidelines for image acquisition, data analysis, and interpretation of results. |

To conclude, by addressing these limitations and focusing on the recommendations, non-linear optical techniques could become a truly promising, more practical, and effective tool for cancer detection implemented in clinical settings in the near future.

Funding: This research received no external funding.

Institutional Review Board Statement: Not applicable.

Informed Consent Statement: Not applicable.

Data Availability Statement: Not applicable.

Conflicts of Interest: The author declares no conflicts of interest.

References

- Gospodarowicz, M.; O’Sullivan, B. Prognostic factors in cancer. *Semin. Surg. Oncol.* **2003**, *21*, 13–18. [[CrossRef](#)] [[PubMed](#)]
- DeBerardinis, R.J.; Chandel, N.S. Fundamentals of cancer metabolism. *Sci. Adv.* **2016**, *2*, e1600200. [[CrossRef](#)] [[PubMed](#)]
- Winkler, J.; Abisoye-Ogunniyan, A.; Metcalf, K.J.; Werb, Z. Concepts of extracellular matrix remodelling in tumour progression and metastasis. *Nat. Commun.* **2020**, *11*, 5120. [[CrossRef](#)] [[PubMed](#)]
- Jones, R.R.; Hooper, D.C.; Zhang, L.; Wolverson, D.; Valev, V.K. Raman Techniques: Fundamentals and Frontiers. *Nanoscale Res. Lett.* **2019**, *14*, 231. [[CrossRef](#)] [[PubMed](#)]
- Larson, A. Multiphoton microscopy. *Nat. Photon.* **2011**, *5*, 1. [[CrossRef](#)]
- Schenke-Layland, K. Non-invasive multiphoton imaging of extracellular matrix structures. *J. Biophotonics* **2008**, *1*, 451–462. [[CrossRef](#)]
- Hu, F.; Shi, L.; Min, W. Biological imaging of chemical bonds by stimulated Raman scattering microscopy. *Nat. Methods* **2019**, *16*, 830–842. [[CrossRef](#)]
- Van Steenbergen, V.; Boesmans, W.; Li, Z.; de Coene, Y.; Vints, K.; Baatsen, P.; Dewachter, I.; Ameloot, M.; Clays, K.; Berghe, P.V. Molecular understanding of label-free second harmonic imaging of microtubules. *Nat. Commun.* **2019**, *10*, 3530. [[CrossRef](#)]
- Szeto, H.H.; Schiller, P.W.; Zhao, K.; Luo, G. Fluorescent dyes alter intracellular targeting and function of cell-penetrating tetrapeptides. *FASEB J.* **2004**, *19*, 118–120. [[CrossRef](#)]
- Jhan, J.-W.; Chang, W.-T.; Chen, H.-C.; Lee, Y.T.; Wu, M.F.; Chen, C.H.; Liau, I. Integrated multiple multi-photon imaging and Raman spectroscopy for characterizing structure-constituent correlation of tissues. *Opt. Express* **2008**, *16*, 16431–16441. [[CrossRef](#)]
- Quansah, E.; Shaik, T.A.; Çevik, E.; Wang, X.; Höppener, C.; Meyer-Zedler, T.; Krafft, C. Investigating biochemical and structural changes of glycosylated collagen using multimodal multiphoton imaging, Raman spectroscopy, and atomic force microscopy. *Anal. Bioanal. Chem.* **2023**, *415*, 6257–6267. [[CrossRef](#)] [[PubMed](#)]
- Kauffmann, T.H.; Kokanyan, N.; Fontana, M.D. Use of Stokes and anti-Stokes Raman scattering for new applications. *J. Raman Spectrosc.* **2018**, *50*, 418–424. [[CrossRef](#)]

13. Griffiths, D.J. *Introduction to Electrodynamics*, 3rd ed.; Pearson Education Dorling Kindersley: Glenview, IL, USA, 2007; ISBN 81-7758-293-3.
14. Qi, Y.F.; Liu, Y.H.; Liu, D.M. Research progress on application of Raman spectroscopy in tumor diagnosis. *Laser Optoelectron. Prog.* **2020**, *57*, 220001.
15. Ilchenko, O.; Pilhun, Y.; Kutsyk, A. Towards Raman imaging of centimeter scale tissue areas for real-time opto-molecular visualization of tissue boundaries for clinical applications. *Light Sci. Appl.* **2022**, *11*, 143. [[CrossRef](#)] [[PubMed](#)]
16. Auner, G.W.; Koya, S.K.; Huang, C.; Broadbent, B.; Trexler, M.; Auner, Z.; Elias, A.; Curtin Mehne, K.; Brusatori, M.A. Applications of Raman spectroscopy in cancer diagnosis. *Cancer Metastasis Rev.* **2018**, *37*, 691–717. [[CrossRef](#)]
17. Hollon, T.; Orringer, D.A. Label-free brain tumor imaging using Raman-based methods. *J. Neuro-Oncol.* **2021**, *151*, 393–402. [[CrossRef](#)]
18. Haka, A.S.; Shafer-Peltier, K.E.; Fitzmaurice, M.; Crowe, J.; Dasari, R.R.; Feld, M.S. Diagnosing breast cancer by using Raman spectroscopy. *Proc. Natl. Acad. Sci. USA* **2005**, *102*, 12371–12376. [[CrossRef](#)]
19. Hanna, K.; Krzoska, E.; Shaaban, A.M.; Muirhead, D.; Abu-Eid, R.; Speirs, V. Raman spectroscopy: Current applications in breast cancer diagnosis, challenges and future prospects. *Br. J. Cancer* **2021**, *126*, 1125–1139. [[CrossRef](#)] [[PubMed](#)]
20. Santos, I.P.; Barroso, E.M.; Bakker Schut, T.C.; Caspers, P.J.; van Lanschot, C.G.F.; Choi, D.-H.; van der Kamp, M.F.; Smits, R.W.H.; van Doorn, R.; Verdijk, R.M.; et al. Raman spectroscopy for cancer detection and cancer surgery guidance: Translation to the clinics. *Analyst* **2017**, *142*, 3025–3047. [[CrossRef](#)]
21. Kong, K.; Rowlands, C.J.; Varma, S.; Perkins, W.; Leach, I.H.; Koloydenko, A.A.; Williams, H.C.; Notingher, I. Diagnosis of tumors during tissue-conserving surgery with integrated autofluorescence and Raman scattering microscopy. *Proc. Natl. Acad. Sci. USA* **2013**, *110*, 15189–15194.
22. Xu, J.; Yu, T.; Zois, C.E.; Cheng, J.-X.; Tang, Y.; Harris, A.L.; Huang, W.E. Unveiling Cancer Metabolism through Spontaneous and Coherent Raman Spectroscopy and Stable Isotope Probing. *Cancers* **2021**, *13*, 1718. [[CrossRef](#)] [[PubMed](#)]
23. Romero, G.; Rojas, E.; Estrela-Lopis, I.; Donath, E.; Moya, S.E. Spontaneous confocal Raman microscopy—a tool to study the uptake of nanoparticles and carbon nanotubes into cells. *Nanoscale Res. Lett.* **2011**, *6*, 429. [[CrossRef](#)] [[PubMed](#)]
24. Nandakumar, P.; Kovalev, A.; Volkmer, A. Vibrational imaging based on stimulated Raman scattering microscopy. *New J. Phys.* **2009**, *11*, 033026. [[CrossRef](#)]
25. Freudiger, C.W.; Min, W.; Saar, B.G.; Lu, S.; Holtom, G.R.; He, C.; Tsai, J.C.; Kang, J.X.; Xie, X.S. Label-free biomedical imaging with high sensitivity by stimulated Raman scattering microscopy. *Science* **2008**, *322*, 1857–1861. [[CrossRef](#)]
26. Zhu, M.; Chen, X.; Chi, M.; Wu, Y.; Zhang, M.; Gao, S. Spontaneous-stimulated Raman co-localization dual-modal analysis approach for efficient identification of tumor cells. *Talanta* **2024**, *277*, 126297. [[CrossRef](#)]
27. Ni, H.; Dessai, C.P.; Lin, H.; Wang, W.; Chen, S.; Yuan, Y.; Ge, X.; Ao, J.; Vild, N.; Cheng, J.-X. High-content stimulated Raman histology of human breast cancer. *Theranostics* **2024**, *14*, 1361–1370. [[CrossRef](#)]
28. Ji, M.; Lewis, S.; Camelo-Piragua, S.; Ramkissoon, S.H.; Snuderl, M.; Venneti, S.; Fisher-Hubbard, A.; Garrard, M.; Fu, D.; Wang, A.C.; et al. Detection of human brain tumor infiltration with quantitative stimulated Raman scattering microscopy. *Sci. Transl. Med.* **2015**, *7*, 309ra163. [[CrossRef](#)]
29. Saar, B.G.; Freudiger, C.W.; Reichman, J.; Stanley, C.M.; Holtom, G.R.; Xie, X.S. Video-Rate Molecular imaging in vivo with stimulated Raman scattering. *Science* **2010**, *330*, 1368–1370. [[CrossRef](#)] [[PubMed](#)]
30. Reinecke, D.; von Spreckelsen, N.; Mawrin, C.; Ion-Margineanu, A.; Fürtjes, G.; Jünger, S.T.; Khalid, F.; Freudiger, C.W.; Timmer, M.; Ruge, M.I.; et al. Novel rapid intraoperative qualitative tumor detection by a residual convolutional neural network using label-free stimulated Raman scattering microscopy. *Acta Neuropathol. Commun.* **2022**, *10*, 109. [[CrossRef](#)]
31. Evans, C.L.; Xie, X.S. Coherent Anti-Stokes Raman Scattering Microscopy: Chemical Imaging for Biology and Medicine. *Annu. Rev. Anal. Chem.* **2008**, *1*, 883–909. [[CrossRef](#)]
32. Zumbusch, A.; Holtom, G.R.; Xie, X.S. Three-dimensional vibrational imaging by coherent anti-Stokes Raman scattering. *Phys. Rev. Lett.* **1999**, *82*, 4142–4145. [[CrossRef](#)]
33. Gachet, D.; Billard, F.; Rigneault, H. Background-free coherent anti-Stokes Raman spectroscopy near transverse interfaces: A vectorial study. *J. Opt. Soc. Am. B* **2008**, *25*, 1655–1666. [[CrossRef](#)]
34. Heuke, S.; Rigneault, H. Coherent Stokes Raman scattering microscopy (CSRS). *Nat. Commun.* **2023**, *14*, 3337. [[CrossRef](#)] [[PubMed](#)]
35. Vito, G.M.; Bifone, A.; Piazza, V. Rotating-polarization CARS microscopy: Combining chemical and molecular orientation sensitivity. *Opt. Express* **2012**, *20*, 29369–29377. [[CrossRef](#)]
36. Li, S.; Li, Y.; Yi, R.; Liu, L.; Qu, J. Coherent Anti-Stokes Raman Scattering Microscopy and Its Applications. *Front. Phys.* **2020**, *8*, 598420. [[CrossRef](#)]
37. McCullagh, E.A.; Polog, S.; Stich, D.; Moldovan, R.; Klug, A. Coherent Anti-Stokes Raman Spectroscopy (CARS) Application for Imaging Myelination in Brain Slices. *J. Vis. Exp.* **2022**, *185*, e64013. [[CrossRef](#)]
38. Le, T.T.; Huff, T.B.; Cheng, J.-X. Coherent anti-Stokes Raman scattering imaging of lipids in cancer metastasis. *BMC Cancer* **2009**, *9*, 42. [[CrossRef](#)]
39. Mitra, R.; Chao, O.; Urasaki, Y.; Goodman, O.B.; Le, T.T. Detection of lipid-rich prostate circulating tumour cells with coherent anti-stokes Raman scattering microscopy. *BMC Cancer* **2012**, *12*, 540. [[CrossRef](#)] [[PubMed](#)]
40. Zeng, J.; Zhao, W.; Yue, S. Coherent Raman Scattering Microscopy in Oncology Pharmacokinetic Research. *Front. Pharmacol.* **2021**, *12*, 630167. [[CrossRef](#)]

41. Vernuccio, F.; Vanna, R.; Ceconello, C.; Bresci, A.; Manetti, F.; Sorrentino, S.; Ghislanzoni, S.; Lambertucci, F.; Motiño, O.; Martins, I.; et al. Full-Spectrum CARS Microscopy of Cells and Tissues with Ultrashort White-Light Continuum Pulses. *J. Phys. Chem. B* **2023**, *127*, 4733–4745. [[CrossRef](#)]
42. Williams, R.M.; Zipfel, W.R.; Webb, W.W. Multiphoton microscopy in biological research. *Curr. Opin. Chem. Biol.* **2001**, *5*, 603–608. [[CrossRef](#)]
43. Stringari, C.; Abdeladim, L.; Malkinson, G.; Mahou, P.; Solinas, X.; Lamarre, I.; Brizion, S.; Galey, J.-B.; Supatto, W.; Legouis, R.; et al. Multicolor two-photon imaging of endogenous fluorophores in living tissues by wavelength mixing. *Sci. Rep.* **2017**, *7*, 3792. [[CrossRef](#)] [[PubMed](#)]
44. Vergen, J.; Hecht, C.; Zholudeva, L.V.; Marquardt, M.M.; Hallworth, R.; Nichols, M.G. Metabolic imaging using two-photon excited NADH intensity and fluorescence lifetime imaging. *Microsc. Microanal.* **2012**, *18*, 761–770. [[CrossRef](#)] [[PubMed](#)]
45. Centonze, V.E.; White, J.G. Multiphoton excitation provides optical sections from deeper within scattering specimens than Confocal imaging. *Biophys. J.* **1998**, *75*, 2015–2024. [[CrossRef](#)]
46. Denk, W.; Strickler, J.H.; Webb, W.W. Two-Photon Laser Scanning Fluorescence Microscopy. *Science* **1990**, *248*, 73–76. [[CrossRef](#)]
47. Helmchen, F.; Denk, W. Deep tissue two-photon microscopy. *Nat. Methods* **2005**, *2*, 932–940. [[CrossRef](#)]
48. Denk, W.; Delaney, K.; Gelperin, A.; Kleinfeld, D.; Strowbridge, B.; Tank, D.; Yuste, R. Anatomical and functional imaging of neurons using 2-photon laser scanning microscopy. *J. Neurosci. Methods* **1994**, *54*, 151–162. [[CrossRef](#)] [[PubMed](#)]
49. Bousso, P.; Bhakta, N.R.; Lewis, R.S.; Robey, E. Dynamics of thymocyte-stromal cell interactions visualized by two-photon microscopy. *Science* **2002**, *296*, 1876–1880. [[CrossRef](#)]
50. Lu, Z.; Zuo, S.; Shi, M.; Fan, J.; Xie, J.; Xiao, G.; Yu, L.; Wu, J.; Dai, Q. Long-term intravital subcellular imaging with confocal scanning light-field microscopy. *Nat. Biotechnol.* **2024**, 38802562. [[CrossRef](#)]
51. Jun, L.I.U. Two-photon microscopy in pre-clinical and clinical cancer research. *Front. Optoelectron.* **2015**, *8*, 141–151.
52. Alzeeb, G.; Dubreuil, M.; Arzur, D.; Rivet, S.; Corcos, L.; Le Grand, Y.; Le Jossic-Corcos, C. Gastric cancer multicellular spheroid analysis by two-photon microscopy. *Biomed. Opt. Express* **2022**, *13*, 3120–3130. [[CrossRef](#)] [[PubMed](#)]
53. Noh, C.-K.; Lim, C.S.; Lee, G.H.; Cho, M.K.; Lee, H.W.; Roh, J.; Kim, Y.B.; Lee, E.; Park, B.; Kim, H.M.; et al. A Diagnostic Method for Gastric Cancer Using Two-Photon Microscopy with Enzyme-Selective Fluorescent Probes: A Pilot Study. *Front. Oncol.* **2021**, *11*, 634219. [[CrossRef](#)]
54. Yang, D.; Liu, J.; Qian, H.; Zhuang, Q. Cancer-associated fibroblasts: From basic science to anticancer therapy. *Exp. Mol. Med.* **2023**, *55*, 1322–1332. [[CrossRef](#)]
55. Franchi-Mendes, T.; Lopes, N.; Brito, C. Heterotypic Tumor Spheroids in Agitation-Based Cultures: A Scaffold-Free Cell Model That Sustains Long-Term Survival of Endothelial Cells. *Front. Bioeng. Biotechnol.* **2021**; *9*, 649949.
56. Li, L.; Hong, S.; Kang, D.; Huang, X.; Zhang, S.; Zhan, Z.; Zhou, Y.; Chen, J. Two-photon imaging reveals histopathological changes in gastric tumor microenvironment induced by neoadjuvant treatment. *Biomed. Opt. Express* **2023**, *14*, 5085–5096. [[CrossRef](#)]
57. Hong, S.T.; Kim, T.H.; Choi, J.W.; Park, S.J.; Kwon, S.A.; Paik, K.C.; Han, M.S.; Kim, E.S.; Chun, H.J.; Heo, J.N.; et al. Two-Photon Probes for pH: Detection of Human Colon Cancer using Two-Photon Microscopy. *Anal. Chem.* **2017**, *89*, 9830–9835. [[CrossRef](#)] [[PubMed](#)]
58. Kwiatkowski, S.; Knap, B.; Przystupski, D.; Saczko, J.; Kędzierska, E.; Knap-Czop, K.; Kotlińska, J.; Michel, O.; Kotowski, K.; Kulbacka, J. Photodynamic therapy-mechanisms, photosensitizers and combinations. *Biomed. Pharmacother.* **2018**, *106*, 1098–1107. [[CrossRef](#)]
59. Benninger, R.K.; Piston, D.W. Two-photon excitation microscopy for the study of living cells and tissues. *Curr. Protoc. Cell Biol.* **2013**, *59*, 4.11.1–4.11.24. [[CrossRef](#)]
60. Juvekar, V.; Lee, D.J.; Park, T.G.; Samanta, R.; Kasar, P.; Kim, C.; Rotermund, F.; Kim, H.M. Two-photon excitation photosensitizers for photodynamic therapy: From small-molecules to nano-complex systems. *Coord. Chem. Rev.* **2024**, *506*, 215711. [[CrossRef](#)]
61. Jung, H.S.; Kim, H.J. Definitive surgery and intraoperative photodynamic therapy for locally advanced non-small cell lung cancer: A case report. *World J. Surg. Oncol.* **2022**, *20*, 265. [[CrossRef](#)]
62. Rodrigues, J.A.; Correia, J.H. Photodynamic Therapy for Colorectal Cancer: An Update and a Look to the Future. *Int. J. Mol. Sci.* **2023**, *24*, 12204. [[CrossRef](#)]
63. Xu, C.; Law, S.K.; Leung, A.W.N. Comparison of the Differences between Two-Photon Excitation, Upconversion, and Conventional Photodynamic Therapy on Cancers in In Vitro and In Vivo Studies. *Pharmaceuticals* **2024**, *17*, 663. [[CrossRef](#)] [[PubMed](#)]
64. Starkey, J.R.; Rebane, A.K.; Drobizhev, M.A.; Meng, F.; Gong, A.; Elliott, A.; McInerney, K.; Spangler, C.W. New Two-Photon Activated Photodynamic Therapy Sensitizers Induce Xenograft Tumor Regressions after Near-IR Laser Treatment through the Body of the Host Mouse. *Clin. Cancer Res.* **2008**, *14*, 6564–6573. [[CrossRef](#)] [[PubMed](#)]
65. Bower, A.J.; Li, J.; Chaney, E.J.; Marjanovic, M.; Spillman, D.R.; Boppart, S.A. High-speed imaging of transient metabolic dynamics using two-photon fluorescence lifetime imaging microscopy. *Optica* **2018**, *5*, 1290–1296. [[CrossRef](#)] [[PubMed](#)]
66. Ranawat, H.; Pal, S.; Mazumder, N. Recent trends in two-photon auto-fluorescence lifetime imaging (2P-FLIM) and its biomedical applications. *Biomed. Eng. Lett.* **2019**, *9*, 293–310. [[CrossRef](#)]
67. Liang, W.; Chen, D.; Guan, H.; Park, H.C.; Li, K.; Li, A.; Li, M.J.; Gannot, I.; Li, X. Label-Free Metabolic Imaging In Vivo by Two-Photon Fluorescence Lifetime Endomicroscopy. *ACS Photonics* **2022**, *9*, 4017–4029. [[CrossRef](#)]
68. Karrobi, K.; Tank, A.; Fuzail, M.A.; Kalidoss, M.; Tilbury, K.; Zaman, M.; Ferruzzi, J.; Roblyer, D. Fluorescence Lifetime Imaging Microscopy (FLIM) reveals spatial-metabolic changes in 3D breast cancer spheroids. *Sci. Rep.* **2023**, *13*, 3624. [[CrossRef](#)]

69. Sundström, V. Femtobiology. *Annu. Rev. Phys. Chem.* **2008**, *59*, 53–77. [[CrossRef](#)]
70. Berera, R.; van Grondelle, R.; Kennis, J.T.M. Ultrafast transient absorption spectroscopy: Principles and application to photosynthetic systems. *Photosynth. Res.* **2009**, *101*, 105–118. [[CrossRef](#)]
71. Zhu, Y.; Cheng, J.-X. Transient absorption microscopy: Technological innovations and applications in materials science and life science. *J. Chem. Phys.* **2020**, *152*, 020901. [[CrossRef](#)]
72. Wang, E.; Whitcomb, L.A.; Chicco, A.J.; Wilson, J.W. Transient absorption spectroscopy and imaging of redox in muscle mitochondria. *Biomed. Opt. Express* **2022**, *13*, 2103–2116. [[CrossRef](#)]
73. Zhang, S.; Wang, J.; Wang, Z.; Shao, M.; Zhang, C.; Chen, X.; Sun, J.; Kwok, R.T.K.; Lam, J.W.Y.; Tang, B.Z. Study of transient absorption spectroscopy of a D- π -A structure aggregation-induced emission luminogen and its photodynamic therapy application. *J. Mater. Chem. B* **2024**, *12*, 8349–8356. [[CrossRef](#)] [[PubMed](#)]
74. Xin, L.; Luo, Z.; Liu, X.; Huang, Z. Unveiling the Spatiotemporal and Dose Responses within a Single Live Cancer Cell to Photo-switchable Upconversion Nanoparticle Therapeutics Using Hybrid Hyperspectral Stimulated Raman Scattering and Transient Absorption Microscopy. *Anal. Chem.* **2024**, *96*, 6148–6157. [[CrossRef](#)]
75. Tanzer, M.L. Current concepts of extracellular matrix. *J. Orthop. Sci.* **2006**, *11*, 326–331. [[CrossRef](#)] [[PubMed](#)]
76. Rozario, T.; DeSimone, D.W. The extracellular matrix in development and morphogenesis: A dynamic view. *Dev. Biol.* **2010**, *341*, 126–140. [[CrossRef](#)]
77. James, D.S.; Campagnola, P.J. Recent Advancements in Optical Harmonic Generation Microscopy: Applications and Perspectives. *BME Front.* **2021**, *2021*, 3973857. [[CrossRef](#)]
78. LaComb, R.; Nadiarnykh, O.; Townsend, S.S.; Campagnola, P.J. Phase Matching Considerations in Second Harmonic Generation from Tissues: Effects on Emission Directionality, Conversion Efficiency and Observed Morphology. *Opt. Commun.* **2007**, *281*, 1823–1832. [[CrossRef](#)]
79. Boyd, R.W. *Nonlinear Optics*; Academic Press: Cambridge, MA, USA, 1992.
80. Williams, R.M.; Zipfel, W.R.; Webb, W.W. Interpreting second-harmonic generation images of collagen I fibrils. *Biophys. J.* **2005**, *88*, 1377–1386. [[CrossRef](#)] [[PubMed](#)]
81. Weigel, B.; Bakker, G.-J.; Friedl, P. Third harmonic generation microscopy of cells and tissue organization. *J. Cell Sci.* **2016**, *129*, 245–255. [[CrossRef](#)]
82. Farrar, M.J.; Wise, F.W.; Fetcho, J.R.; Schaffer, C.B. In Vivo imaging of myelin in the vertebrate central nervous system using third harmonic generation microscopy. *Biophys. J.* **2011**, *100*, 1362–1371. [[CrossRef](#)]
83. Popova, N.V.; Jücker, M. The Functional Role of Extracellular Matrix Proteins in Cancer. *Cancers* **2022**, *14*, 238. [[CrossRef](#)]
84. Kular, J.K.; Basu, S.; Sharma, R.I. The extracellular matrix: Structure, composition, age-related differences, tools for analysis and applications for tissue engineering. *J. Tissue Eng.* **2014**, *5*, 2041731414557112. [[CrossRef](#)]
85. Aghigh, A.; Bancelin, S.; Rivard, M.; Pinsard, M.; Ibrahim, H.; Légaré, F. Second harmonic generation microscopy: A powerful tool for bio-imaging. *Biophys. Rev.* **2023**, *15*, 43–70. [[CrossRef](#)] [[PubMed](#)]
86. Mohler, W.; Millard, A.C.; Campagnola, P.J. Second harmonic generation imaging of endogenous structural proteins. *Methods* **2003**, *29*, 97–109. [[CrossRef](#)]
87. Jiang, J.; Yuste, R. Second-Harmonic generation imaging of membrane potential with photon counting. *Microsc. Microanal.* **2008**, *14*, 526–531. [[CrossRef](#)] [[PubMed](#)]
88. Wallace, S.J.; Morrison, J.L.; Botting, K.J.; Kee, T.W. Second-harmonic generation and two-photon-excited autofluorescence microscopy of cardiomyocytes: Quantification of cell volume and myosin filaments. *J. Biomed. Opt.* **2008**, *13*, 064018. [[CrossRef](#)] [[PubMed](#)]
89. Liu, J.; Jin, Y.; Liu, H.; Wang, F.; Deng, X. The forward and backward second-harmonic generation from crystallized collagen fibre with tightly focused linearly polarized beams. *J. Opt.* **2012**, *14*, 055301. [[CrossRef](#)]
90. Keikhosravi, A.; Bredfeldt, J.S.; Sagar, A.K.; Eliceiri, K.W. Second-harmonic generation imaging of cancer. *Methods Cell Biol.* **2014**, *123*, 531–546.
91. Mierke, C.T. The matrix environmental and cell mechanical properties regulate cell migration and contribute to the invasive phenotype of cancer cells. *Rep Prog Phys.* **2019**, *82*, 064602. [[CrossRef](#)]
92. Song, K.; Yu, Z.; Zu, X.; Li, G.; Hu, Z.; Xue, Y. Collagen Remodeling along Cancer Progression Providing a Novel Opportunity for Cancer Diagnosis and Treatment. *Int. J. Mol. Sci.* **2022**, *23*, 10509. [[CrossRef](#)]
93. Desa, D.E.; Wu, W.; Brown, R.M.; Brown, E.B., 4th; Hill, R.L.; Turner, B.M.; Brown, E.B., 3rd. Second-Harmonic Generation Imaging Reveals Changes in Breast Tumor Collagen Induced by Neoadjuvant Chemotherapy. *Cancers* **2022**, *14*, 857. [[CrossRef](#)]
94. Venning, F.A.; Wullkopf, L.; Erler, J.T. Targeting ECM Disrupts Cancer Progression. *Front. Oncol.* **2015**, *5*, 224. [[CrossRef](#)] [[PubMed](#)]
95. Nejm, Z.; Navarro, L.; Morin, C.; Badel, P. Quantitative analysis of second harmonic generated images of collagen fibers: A review. *Res. Biomed. Eng.* **2022**, *39*, 273–295. [[CrossRef](#)]
96. Ávila, F.J.; Bueno, J.M. Analysis and quantification of collagen organization with the structure tensor in second harmonic microscopy images of ocular tissues. *Appl. Opt.* **2015**, *54*, 9848–9854. [[CrossRef](#)] [[PubMed](#)]
97. Bueno, J.M.; Ávila, F.J.; Hristu, R.; Stanciu, S.G.; Eftimie, L.; Stanciu, G.A. Objective analysis of collagen organization in thyroid nodule capsules using second harmonic generation microscopy images and the Hough transform. *Appl. Opt.* **2020**, *59*, 6925. [[CrossRef](#)]

98. Alizadeh, M.; Ghotbi, M.; Loza-Alvarez, P.; Merino, D. Comparison of Different Polarization Sensitive Second Harmonic Generation Imaging Techniques. *Methods Protoc.* **2019**, *2*, 49. [[CrossRef](#)]
99. Yu, W.; Li, X.; Wang, B.; Li, Y.; Shen, B.; Qu, J.; Liu, L. Nonlinear polarization tensor measurement with a vectorial complex field in second-harmonic-generation microscopy. *Phys. Rev. A* **2023**, *107*, 013505. [[CrossRef](#)]
100. Golaraei, A.; Kontenis, L.; Cisek, R.; Tokarz, D.; Done, S.J.; Wilson, B.C.; Barzda, V. Changes of collagen ultrastructure in breast cancer tissue determined by second-harmonic generation double Stokes-Mueller polarimetric microscopy. *Biomed. Opt. Express* **2016**, *7*, 4054–4068. [[CrossRef](#)]
101. Tokarz, D.; Cisek, R.; Joseph, A.; Asa, S.L.; Wilson, B.C.; Barzda, V. Characterization of pathological thyroid tissue using polarization-sensitive second harmonic generation microscopy. *Mod. Pathol.* **2020**, *100*, 1280–1287. [[CrossRef](#)]
102. Hompland, T.; Erikson, A.; Lindgren, M.; Lindmo, T.; Davies, C.d.L. Second-Harmonic Generation in Collagen as a Potential Cancer Diagnostic Parameter. *J. Biomed. Opt.* **2008**, *13*, 054050. [[CrossRef](#)]
103. Rouède, D.; Schaub, E.; Bellanger, J.-J.; Ezan, F.; Scimeca, J.-C.; Baffet, G.; Tiaho, F. Determination of Extracellular Matrix Collagen Fibril Architectures and Pathological Remodeling by Polarization Dependent Second Harmonic Microscopy. *Sci. Rep.* **2017**, *7*, 12197. [[CrossRef](#)]
104. Ambekar, R.; Lau, T.-Y.; Walsh, M.; Bhargava, R.; Toussaint, K.C. Quantifying Collagen Structure in Breast Biopsies Using Second-Harmonic Generation Imaging. *Biomed. Opt. Express* **2012**, *3*, 2021–2035. [[CrossRef](#)] [[PubMed](#)]
105. Lin, J.; Pan, S.; Zheng, W.; Huang, Z. Polarization-Resolved Second-Harmonic Generation Imaging for Liver Fibrosis Assessment without Labeling. *Appl. Phys. Lett.* **2013**, *103*, 173701. [[CrossRef](#)]
106. Watanabe, T.; Thayil, A.; Jesacher, A.; Grieve, K.; Debarre, D.; Wilson, T.; Booth, M.; Srinivas, S. Characterisation of the dynamic behaviour of lipid droplets in the early mouse embryo using adaptive harmonic generation microscopy. *BMC Cell Biol.* **2010**, *11*, 38. [[CrossRef](#)] [[PubMed](#)]
107. Müller; Squier; Wilson; Brakenhoff 3D microscopy of transparent objects using third-harmonic generation. *J. Microsc.* **1998**, *191*, 266–274. [[CrossRef](#)] [[PubMed](#)]
108. Chu, S.W.; Chen, S.Y.; Chern, G.W.; Tsai, T.H.; Chen, Y.C.; Lin, B.L.; Sun, C.K. Studies of chi(2)/chi(3) tensors in submicron-scaled bio-tissues by polarization harmonics optical microscopy. *Biophys. J.* **2004**, *86*, 3914–3922. [[CrossRef](#)] [[PubMed](#)]
109. Gavgiotaki, E.; Filippidis, G.; Tsafas, V.; Bovasianos, S.; Kenanakis, G.; Georgoulas, V.; Tzardi, M.; Agelaki, S.; Athanassakis, I. Third Harmonic Generation microscopy distinguishes malignant cell grade in human breast tissue biopsies. *Sci. Rep.* **2020**, *10*, 11055. [[CrossRef](#)]
110. Gavgiotaki, E.; Filippidis, G.; Markomanolaki, H.; Kenanakis, G.; Agelaki, S.; Georgoulas, V.; Athanassakis, I. Distinction between breast cancer cell subtypes using third harmonic generation microscopy. *J. Biophotonics* **2016**, *10*, 1152–1162. [[CrossRef](#)]
111. Ardakani, A.A.; Ghader, A.; Asgari, H.; Keshavarz, M.; Tazehmahalleh, F.E.; Ara, M.H.M.; Malekzadeh, M.; Ghaznavi, H.; Shakeri-Zadeh, A. The capability of nonlinear optical characteristics as a predictor for cellular uptake of nanoparticles and cell damage. *Photodiagnosis Photodyn. Ther.* **2019**, *27*, 442–448. [[CrossRef](#)]
112. Combes, G.F.; Vučković, A.-M.; Bakulić, M.P.; Antoine, R.; Bonačić-Koutecky, V.; Trajković, K. Nanotechnology in Tumor Biomarker Detection: The Potential of Liganded Nanoclusters as Nonlinear Optical Contrast Agents for Molecular Diagnostics of Cancer. *Cancers* **2021**, *13*, 4206. [[CrossRef](#)]
113. Sun, L.; Liu, H.; Ye, Y.; Lei, Y.; Islam, R.; Tan, S.; Tong, R.; Miao, Y.-B.; Cai, L. Smart nanoparticles for cancer therapy. *Signal Transduct. Target. Ther.* **2023**, *8*, 418. [[CrossRef](#)]
114. Aneesa, V.M.; Safna, K.P.; Hussan, S.; Lekshmi, S.; Babu, T.D.; Muraleedharan, K. Analysis of non-linear optical properties of phytochemical photosensitizers in cancer photodynamic therapy by quantum computational. *Results Chem.* **2024**, *8*, 101580. [[CrossRef](#)]
115. Hoque, E.; Biswas, M.K.; Hossain, M.; Bhattacharja, S.; Hasan, K.M.E.; Sharafuddin, S.M.; Das, S.K.; Haque, Y. Nonlinear optical phase shift in blood plasmas for neoplasia diagnosis. *Opt. Express* **2023**, *31*, 23056–23065. [[CrossRef](#)] [[PubMed](#)]
116. Ghader, A.; Behruzi, M.; Ara, M.H.M.; Ghaznavi, H.; Ardakani, A.A. Nonlinear optical response of cancer cells following conventional and nano-technology based treatment strategies: Results of chemo-, thermo- and radiation therapies. *Photodiagnosis Photodyn. Ther.* **2021**, *37*, 102686. [[CrossRef](#)] [[PubMed](#)]

Disclaimer/Publisher’s Note: The statements, opinions and data contained in all publications are solely those of the individual author(s) and contributor(s) and not of MDPI and/or the editor(s). MDPI and/or the editor(s) disclaim responsibility for any injury to people or property resulting from any ideas, methods, instructions or products referred to in the content.